ORIGINAL

Multiparametric Analysis of Tumor Morphological and Functional MR Parameters Potentially Predicts Local Failure in Pharynx Squamous Cell Carcinoma Patients

Noriyuki Fujima[1, 2], Yukie Shimizu[1], Daisuke Yoshida[1], Satoshi Kano[3], Takatsugu Mizumachi[3], Akihiro Homma[3], Koichi Yasuda[2, 4], Rikiya Onimaru[4], Osamu Sakai[5], Kohsuke Kudo[1, 2], and Hiroki Shirato[2, 4]

[1]Department of Diagnostic and Interventional Radiology, Hokkaido University Hospital, Sapporo, Japan, [2]The Global Station for Quantum Medical Science and Engineering, Global Institution for collaborative research and education, Sapporo, Japan, [3]Department of Otolaryngology-Head and Neck Surgery, Hokkaido University Graduate School of Medicine, Sapporo, Japan, [4]Department of Radiation Medicine, Hokkaido University Graduate School of Medicine, Sapporo, Japan, [5]Departments of Radiology, Otolaryngology-Head and Neck Surgery, and Radiation Oncology, Boston Medical Center, Boston University School of Medicine, Boston, MA, USA

Abstract : Purpose : To predict local control/failure by a multiparametric approach using magnetic resonance (MR)-derived tumor morphological and functional parameters in pharynx squamous cell carcinoma (SCC) patients. Materials and Methods : Twenty-eight patients with oropharyngeal and hypopharyngeal SCCs were included in this study. Quantitative morphological parameters and intratumoral characteristics on T2-weighted images, tumor blood flow from pseudo-continuous arterial spin labeling, and tumor diffusion parameters of three diffusion models from multi-*b*-value diffusion-weighted imaging as well as patients' characteristics were analyzed. The patients were divided into local control/failure groups. Univariate and multiparametric analysis were performed for the patient group division. Results : The value of morphological parameter of 'sphericity' and intratumoral characteristic of 'homogeneity' was revealed respectively significant for the prediction of the local control status in univariate analysis. Higher diagnostic performance was obtained with the sensitivity of 0.8, specificity of 0.75, positive predictive value of 0.89, negative predictive value of 0.6 and accuracy of 0.79 by multiparametric diagnostic model compared to results in the univariate analysis. Conclusion : A multiparametric analysis with MR-derived quantitative parameters may be useful to predict local control in pharynx SCC patients. J. Med. Invest. 68 : 354-361, August, 2021

Keywords **:** *Magnetic Resonance Imaging, Multiparametric Magnetic Resonance Imaging, Squamous Cell Carcinoma of Head and Neck, Treatment Outcome*

INTRODUCTION

Achieving local control with the appropriate methods are treatment goals for patients with head and neck squamous cell carcinomas (SCCs). It would be very helpful if we could predict the treatment outcomes such as local control or failure when treatment decisions are being made, such as type of surgery, selection of chemotherapy (e.g., whether to perform induction chemotherapy), and radiation therapy planning, and also to determine the best post-treatment imaging follow-up strategy. The optimization of patient assessment will lead to truly personalized precision medicine for the best prognosis.

To predict prognoses of patients with SCCs, which are closely related to treatment outcomes, conventionally the TNM stage, tumor size, and histological grade have been used (1-3). In addition to such traditional tumor information, characteristics of tumor morphology and intratumoral heterogeneity have been evaluated by an advanced mathematical approach using conventional imaging by CT, MRI and FDG-PET ; advanced morphological shape characteristics of tumors such as sphericity were indicated to be useful for the prediction of treatment outcomes in head and neck SCC compared to simple tumor size information, whereas intratumoral heterogeneity was also indicated as a prognostic factor in head and neck SCC patients and tumors with high degree of intratumoral heterogeneity demonstrated a tendency for poor prognoses (4, 5). Tumor functional information such as tumor perfusion values was described as an important predictor of the treatment outcome ; lower tumor perfusion was related to poor treatment outcome in these reports, probably because of the relation between tumor hypoxia and lower tumor perfusion (6, 7). In patients with head and neck SCCs, tumor diffusion information was reported to be useful to predict the treatment outcome ; diffusion parameters were suggested to reflect tumor microenvironment such as tumor cell density, and thus enable to evaluate tumor characteristics in greater detail (8, 9). In addition, a non-Gaussian diffusion model such as diffusion kurtosis imaging (DKI) was considered in order to visualize the microstructural complexity (10, 11), which could have a possible relation to the presence of intratumoral necrosis (12). This information was useful for outcome prediction.

These tumor characteristics may provide higher diagnostic accuracy when several of the above-described information is effectively combined rather than using each parameter independently. Multiparametric model, such as machine learning approach, were introduced for the effective selection of several parameters as a type of analysis technique including the field of head and neck oncology (13-15). Effectively combining several tumor characteristics may result in a better diagnostic performance.

Received for publication March 12, 2021 ; accepted August 19, 2021.

Address correspondence and reprint requests to Noriyuki Fujima, Department of Diagnostic and Interventional Radiology, Hokkaido University Hospital, N15, W7, Kita-Ku, Sapporo 060-8638, Japan and Fax : +81-11-706-7876.

We conducted the present study to determine the diagnostic accuracy of magnetic resonance (MR)-derived parameters of tumor morphology, intratumoral characteristics, tumor perfusion, diffusion information, and the multiparametric approach by integrating several of those MR-derived parameters efficiently to predict treatment outcomes in patients with oropharyngeal and hypopharyngeal SCCs. We targeted patients treated with super-selective arterial infusions of cisplatin with concomitant radiotherapy which have become popular for head and neck SCC because of its higher local control rate in advanced cases, including pharynx SCC (16).

PATIENTS AND METHODS

Patients

This retrospective study was approved by our institutional review board, and the requirement to obtain written informed consent was waived. From March 2010 to June 2017, 28 patients with oropharyngeal and hypopharyngeal SCCs referred to our hospital met all of the following inclusion criteria and were included in this study ; (1) had a histopathological diagnosis of SCC in the oropharynx or hypopharynx, (2) received a specific treatment regimen (super-selective arterial infusion of cisplatin with concomitant radiotherapy of total 70 Gy) with curative intent, (3) had undergone an MRI examination including conventional anatomical imaging of T1-weighted images (T1WI), fat-suppressed T2-weighted images (Fs-T2WI), arterial spin labeling (ASL), and multiple *b*-value diffusion-weighted imaging (DWI) before treatment. The patients' characteristics are summarized in Table 1.

To avoid a large variation of treatment regimens that can affect the interpretation of the analysis results, we examined the cases of only the patients who underwent a specific treatment regimen (which did not differ among the patients). The details of this regimen are as follows : an arterial infusion of cisplatin (100–120 mg/m^2 per week for 4 weeks) to the primary tumor's dominant blood supply via a microcatheter, with concurrent radiotherapy of a total of 70 Gy in 35 fractions (16). For the management of any residual mass of neck metastatic lymph nodes after chemoradiation therapy, the patients with resectable neck nodes underwent additional surgical dissection.

MR imaging protocol

All MR scanning was performed using a 3.0-Tesla unit (Achieva TX ; Philips Healthcare, Best, Netherlands) with a 16-channel neurovascular coil. All axial slices were placed in parallel with the anterior commissure–posterior commissure line. Conventional MRI sequences of axial FsT2WI were obtained to analyze the tumor morphological and intratumoral heterogeneity parameters. As supportive information, axial T1WI was also used for the evaluation. Pseudo-continuous ASL (pCASL) was conducted for the analysis of the tumor perfusion information. The acquisition of pCASL was performed using multi-shot spin-echo echo-planar imaging to obtain control and labeled images following a previously described protocol (17). In this protocol, the post-labeling delay (PLD) time was set at 1280 ms ; this PLD was a bit shorter compared to the conventional time (typically around 1500-2000 ms) ; however, it was not considered inappropriate when evaluating tumor blood flow because a marked transit delay is frequently not present when assessing malignant tumors. The labeling slab was placed just under the bifurcation of the internal and external carotid arteries. Control images were obtained without the labeling of arterial water, using the same imaging scheme as the labeled images. Multi-*b*-point DWI was also conducted using single-shot spin-echo echo-planar imaging (EPI) with three orthogonal motion-probing gradients following a reported acquisition protocol with 12 *b*-values : 0, 10, 20, 30, 50, 80, 100, 200, 400, 800, 1000, and 2000 s/mm^2 (18, 19) to analyze the tumor microstructural information using DWI-derived parameters. All images were acquired on the basis of the axial plane. The imaging parameters used for the T1WI, T2WI, pCASL, and DWI are summarized in Table 2.

Data analysis

ROI delineation

Each tumor was delineated by a board-certified neuroradiologist with 10 years' experience with a polygonal region-of-interest (ROI) on Fs-T2WI, ASL perfusion images, and DWI *b*0 images. The ROI of the axial Fs-T2WI was first placed, and then the same ROI was delineated with reference to the Fs-T2WI ROI so that the same region was delineated in all images. Manual

Table 1. Patient characteristics

Age	
Median	62 years old
Mean	61.3 years old
Range	41-77 years old
Gender	
Male	24
Female	4
Primary tumor site	
Oropharynx	24
Hypopharynx	4
T-stage	
T1	0
T2	6
T3	4
T4a	15
T4b	3
N-stage	
N0	6
N1	6
N2	16
N3	0
Smoking status	
Tabacco smokers	24
Packs-years	
Median	29 packs-years
Mean	29.5 packs-years
Range	8-94 packs-years
Alcohol use	
Occasional or non-drinker	7
Moderate use (<14 units/week)	3
Heavy use (≥14 units/week)	18
HPV status	
Positive	8
Negative	6
Unknown	14

Table 1 footnote : one unit of alcohol use means 58 g/10 mL ethanol.

correction of the ROI was performed as necessary depending on the degree of image distortion observed in ASL and DWI *b*0 images. For the DWI analysis, the tumor ROI on the *b*0 image was copied on the respective *b*-value images. Any areas of suspected necrosis or cystic lesions were excluded from the ROI. If the tumor extended into two or more slices, all slices were delineated respectively. In addition, the sternocleidomastoid muscle of the healthy side was also delineated with a polygonal ROI on Fs-T2WI to calculate the relative T2WI signal intensity. The example of tumor ROI delineation on Fs-T2WI, ASL and DWI was presented in Figure 1.

Table 2. Imaging parameters

	Basic Sequence	TR (ms)	TE (ms)	FOV (cm)	matrix	slice thickness (mm)	slice gap (mm)	scanning time
T1WI	SE	450	10	24 × 24	512 × 512	5	1.5	2'12
Fs-T2WI	TSE	4500	70	24 × 24	512 × 512	5	1.5	2'06
pCASL	SE-EPI	3619	18	23 × 23	80 × 80	5	1.5	5'11
	Other specific parameters ; labeling duration 1650 ms, PLD 1280 ms, SENSE factor 2.5							
DWI	SE-EPI	4500	64	23 × 23	64 × 64	5	1.5	4'37
	Other specific parameters ; EPI factor 32, SENSE factor 2.0							

Table 2 footnote : TR : repetition time, TE : echo time, FOV : field of view, T1WI : T1 weighted image, SE : spin echo, Fs-T2WI : fat-suppressed T2 weighted image, TSE : turbo spin echo, pCASL : pseudo-continuous arterial spin labeling, SE-EPI : spin-echo echo-planar imaging, PLD : post labeling delay, SENSE : sensitivity encode, DWI : diffusion weighted imaging, EPI : echo planar imaging.

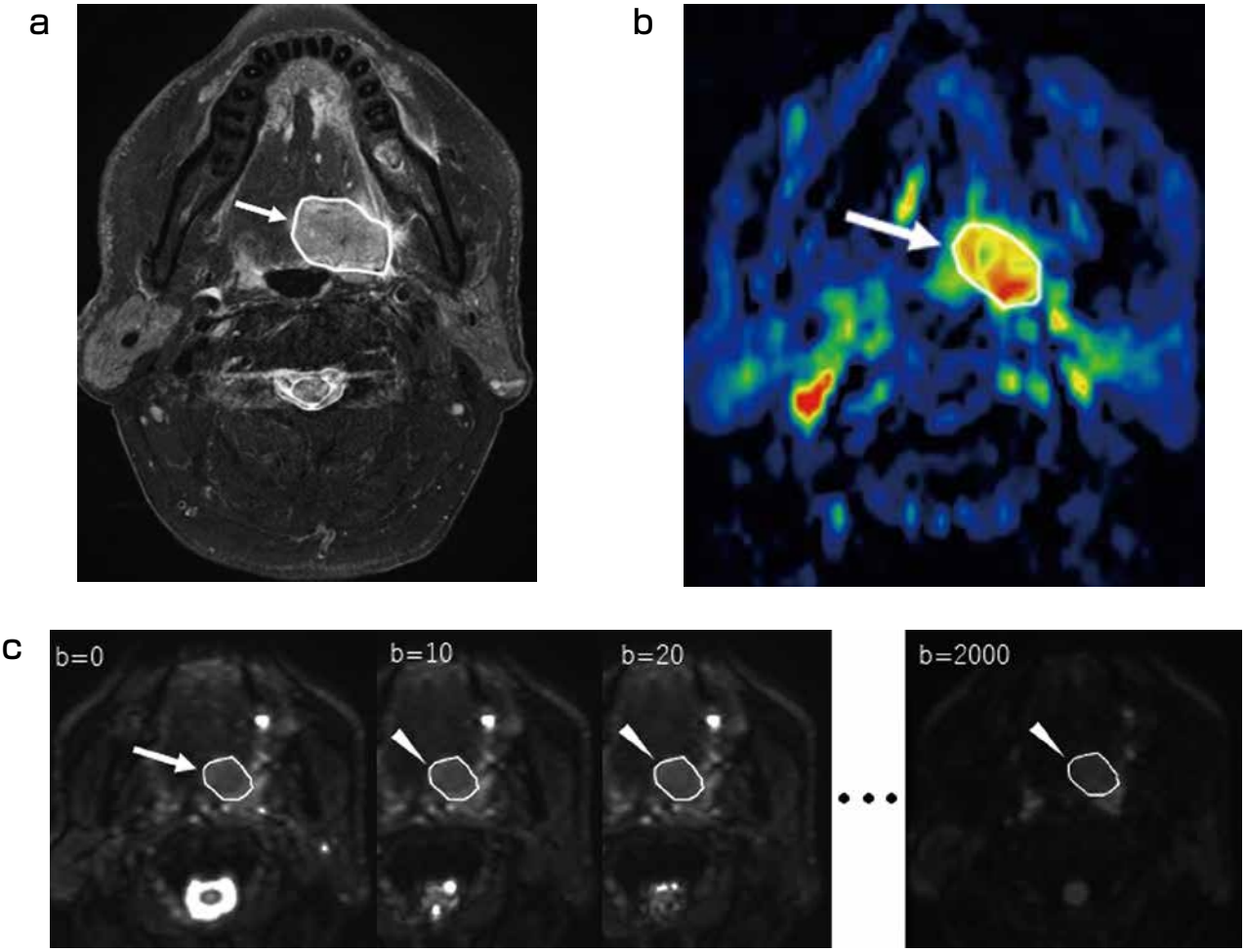

Fig 1. Tumor ROI delineation. Each primary tumor was firstly outlined by a polygonal ROI on Fs-T2WI (a ; arrow). Subsequently, primary tumor on ASL perfusion images (b ; arrow) and b0 images of DWI (c ; arrow) were delineated with reference to the Fs-T2WI ROI so that the same region was outlined among Fs-T2WI, ASL and DWI. For the DWI analysis, the tumor ROI on the *b*0 image was then copied on the EPI of the respective b-values (c ; arrowheads).

Analysis of the Fs-T2WI for morphological and intratumoral data

For the analysis of morphological characteristics, the tumor volume and tumor surface area were directly calculated from the morphological shape, which consisted of all selected tumor voxels in the delineated tumor ROI on Fs-T2WI. The sphericity of each tumor was calculated by a previously reported method (4). For the intra-tumoral characteristics analysis, the relative Fs-T2WI mean signal intensity (= the mean signal on the tumor ROI/the medial pterygoid muscle ROI), the coefficient of variance (CV) in the tumor ROI, and the textural parameters within the ROI were calculated. In the analysis of textural features, the gray-level co-occurrence matrix (GLCM) features were analyzed because GLCM features were reported as the most common and sensitive texture descriptor to calculate lesion heterogeneity in greater detail from the texture data (20). Texture parameters of contrast, correlation, energy and homogeneity were calculated based on a reported method (21). In addition, for the calculation of texture parameters, intensity normalization was performed by remapping the brightness to an 8-bit (from 1 to 256) scale between the minimum and maximum values or within the mean value ± 3 standard deviations of an image (22).

ASL analysis

The tumor blood flow (TBF) was calculated using the pCASL technique from the signal data in ASL subtraction images using a previously described following equation (17) ;

$$f = \frac{\Delta M \lambda R_{1a} \exp(\omega R_{1a})}{2 M_0 \alpha}[1 - \exp(-\gamma R_{1a})]^{-1}$$

where f is the value of TBF, ΔM is the signal difference between pCASL labeled and control images, R_{1a} is the longitudinal relaxation rate of blood (0.67 s^{-1}) (14), γ is the labeling time (1.65 s), ω is the post-labeling delay time (1.28 s), α is the labeling efficiency (0.85), and λ is the blood/tumor-tissue water partition coefficient (1.0 g/mL) (17). M_0 is the equilibrium magnetization of the tumor tissue, which was estimated from the signal intensity in control images. TBF values in each tumor were calculated as the mean TBF value in each tumor's delineated tumor ROI.

DWI analysis

From the diffusion-weighted imaging data, each parameter of mono-exponential function (the apparent diffusion coefficient ; ADC), the bi-exponential function, i.e., the so-called intravoxel incoherent motion (IVIM) (the perfusion fraction f, the fast diffusion coefficient D*, and the slow diffusion coefficient D), and the DKI (kurtosis value K and kurtosis-corrected diffusion coefficient D_k) were calculated. Using the signal intensities of all 12 *b*-values, we calculated the bi-exponential function parameters. Assessments of the ADC and DKI usually target tissue diffusion (except for the perfusion-related signal), and we therefore used the signal intensity of six *b*-values (0, 200, 400, 800, 1000, and 2000 s/mm^2) for the parameter calculations of the ADC and DKI. To perform these parameter calculations, we used the following equations (19) ;

$$\frac{S_{(b)}}{S_0} = e^{-b \cdot ADC} \quad [1]$$

$$\frac{S_{(b)}}{S_0} = f \cdot e^{-b \cdot D^*} + (1 - f) \cdot e^{-b \cdot D} \quad [2]$$

$$\frac{S_{(b)}}{S_0} = \exp\left[- b * D_k + \frac{1}{6} * b^2 * {D_k}^2 * K \right] \quad [3]$$

where $S_{(b)}$ is the signal intensity at the b-value denoted by the subscript, S_0 is the signal intensity at the b-value of 0, and *b* is b-factor in Eqs. [1] to [3]. We fitted the signal intensity of b-values in Eqs. [1] to [3] with least square fitting using the Levenberg-Marquardt algorithm. We used the average signal intensity value in the ROI on each image for the calculation of these diffusion parameters. The self-developed program by MATLAB ver. 2015a (MathWorks, Natick, MA) was used for the above-described calculations.

Clinical assessment for the final diagnosis

In all patients, clinical and radiological follow-ups were performed after the treatment to determine the final diagnosis related to the local control/failure at least 2 years. The follow-up duration was measured from the end of treatment. We assessed whether each patient experience local failure during its whole follow up time. Local failure was determined by the histopathological confirmation of SCC in biopsied or surgically resected tissue, or development of a new mass in the post-treatment site or residual tumor enlargement on follow-up imaging studies.

Statistical analysis based on the univariate and multiparametric approach

For the multiparametric approach, a linear support vector machine (SVM) was used to obtain the best combination of features for the differentiation of local control versus failure groups. For the SVM analysis, a linear kernel and cost parameter (C) of 1 (= default setting) were used. We simply used this default setting to avoid overfitting of the created model. In creating the multiparametric diagnostic model and in evaluating the model accuracy, a leave-one-out cross-validation scheme was used. In this process, the data were divided into 27 training cohorts and one validation cohort ; 28 repetitions of the training and validation analyses with different validation cohorts were performed in a leave-one-out cross-validation scheme. In each training session, feature extraction and SVM model creation were performed. All MR-derived parameters (three morphological characteristics, six intratumoral characteristics, one perfusion parameter, and six diffusion parameters) were first included. Before the feature selection, multicollinearity between respective parameters was assessed in advance with the variance inflation factors (VIFs) (reference value of 10). Parameters that showed multicollinearity to other parameters were subsequently removed. In the feature-selection process, a backward sequential selection to eliminate features was performed. This method was based on an iterative technique in which the starting condition included all of the features. With each iteration, the feature with the least impact on the contribution to the diagnostic performance for the differentiation was eliminated. Features were removed one by one, and the process was repeated until the number of finally selected features was less than or equal to three ; this elimination process was performed to avoid overfitting of the finally established diagnostic model. In each validation session, one validation cohort was diagnosed using the created multiparametric model in the training session. The mean diagnostic accuracy over 28 repetitions was calculated to determine the diagnostic performance that could predict patients with local control/failure.

We also conducted a univariate analysis to compare all MR derived parameters and patients' characteristics (T-stage, N-stage, smoking status, alcohol use and human papillomavirus status) respectively between the patients with and without local control using the Mann-Whitney U-test. In assessing the patients' characteristics, we converted each characteristic into a score as follows : T-stage (T1 = 1, T2 = 2, T3 = 3, T4 = 4), N-stage (N0 = 0, N1 = 1, N2 = 2, N3 = 3), alcohol use (occasional

or non-drinker = 0, moderate use = 1, heavy use = 2) and HPV status (positive = 0, negative or unknown = 1), whereas the pack-years value was directly used in assessing the smoking status. If a significant difference was observed, such parameters were further analyzed by the receiver operating characteristic (ROC) curve analysis, after that, the diagnostic power was determined using the optimal cut-off value determined by the Youden Index.

RESULTS

Eight patients were revealed to have local failure by a clinical assessment. Of these eight patients, local failure was proven in six by a surgical biopsy with the histological demonstration of residual SCC. In the other two patients, a large new lesion was observed by CT images during the follow-up period. The remaining 20 patients were revealed to have achieved local control by clinical observation and imaging studies throughout their follow-up (mean 73.2 months ; range 27–98 months).

In all 28 SCC patients, the analyses of the primary sites were successfully performed. Table 3 summarizes the details of all MR derived parameters (tumor morphological, intratumoral characteristics, the perfusion and diffusion parameters) and patients' characteristics (T-stage, N-stage, smoking status, alcohol

Table 3. Patient characteristics and parameters of the patients with local control and failure

			Treatment outcome		
			Local control	Local failure	P value
Patients' characteristics	T-stage	T1	0	0	0.11
		T2	6	0	
		T3	2	2	
		T4	12	6	
	N-stage	N0	4	2	0.36
		N1	3	3	
		N2	13	3	
		N3	0	0	
	Smoking status	Packs-years	32.9±23.8	20.8±16.7	0.15
	Alcohol use	Occasional or non-drinker	5	2	0.87
		Moderate use	3	0	
		Heavy use	12	6	
	HPV status	Positive	6	1	0.39
		Negative	3	0	
		Unknown	11	7	
Morphological Parameters	Tumor volume (ml)		15.9 ± 7.6	15.3 ± 7.2	0.81
	Surface area (cm^2)		40.8 ± 13	50.1 ± 16.3	0.24
	Sphericity		0.59 ± 0.1	0.45 ± 0.08	0.008*
Intratumoral Characteristics Parameters	Relative mean signal		3.1 ± 0.4	3.1 ± 0.6	0.76
	Coefficient of variance		0.12 ± 0.02	0.13 ± 0.03	0.78
	Contrast		34.8 ± 6.8	37.3 ± 6.5	0.32
	Correlation		0.84 ± 0.05	0.81 ± 0.04	0.34
	Energy ($\times 10^{-3}$)		1.7 ± 0.2	1.5 ± 0.5	0.24
	Homogeneity		0.29 ± 0.03	0.27 ± 0.01	0.03*
Perfusion Parameters	TBF (ml/100g/min)		125.6 ± 17.6	108.7 ± 26.6	0.09
Diffusion Parameters	ADC ($\times 10^{-3}$ mm^2/s)		0.92 ± 0.09	0.89 ± 0.1	0.44
	f ($\times 10^{2}$ %)		0.14 ± 0.04	0.12 ± 0.03	0.18
	D* ($\times 10^{-3}$ mm^2/s)		18.9 ± 6.2	15.2 ± 5.2	0.21
	D ($\times 10^{-3}$ mm^2/s)		0.73 ± 0.09	0.74 ± 0.11	0.65
	K		0.78 ± 0.18	0.82 ± 0.09	0.51
	Dk ($\times 10^{-3}$ mm^2/s)		0.97 ± 0.11	0.94 ± 0.16	0.46

Table 3 footnote : Smoking status and data of all parameters are mean ± standard deviation. TBF : tumor blood flow, ADC : apparent diffusion coefficient, D : slow diffusion coefficient, f : perfusion fraction, D* : fast diffusion coefficient, K : kurtosis value, Dk : kurtosis corrected diffusion coefficient.

use and human papillomavirus status) between the local control and failure groups.

In the multiparametric analysis of the prediction of the local control status, the diagnostic performance (= average of 28 repetitive evaluations in a leave-one-out cross validation scheme) in the training session was as follows : sensitivity, 0.86 ; specificity, 0.82 ; positive predictive value (PPV), 0.92 ; negative predictive value (NPV), 0.7 ; and accuracy, 0.85. Table 4 summarizes the details of selected features and the diagnostic performance in each training session. The diagnostic performance in the validation session was as follows : sensitivity, 0.8 ; specificity, 0.75 ; positive predictive value (PPV), 0.89 ; negative predictive value (NPV), 0.6 ; and accuracy, 0.79.

In a univariate analysis, results in each variable between the patients with and without local control using the Mann-Whitney U-test were also provided in Table 3. The value of sphericity ($p<0.01$) and homogeneity ($p<0.05$) was revealed respectively significant. Respective diagnostic performance of these parameters was determined by ROC curve analysis as follows ; [sphericity] sensitivity of 0.65, specificity of 0.75, PPV of 0.87, NPV of 0.46, and accuracy of 0.68, [homogeneity] sensitivity of 0.7, specificity of 0.63, PPV of 0.82, NPV of 0.45, and accuracy of 0.68. The diagnostic accuracy of these parameters were lower compared to the multiparametric analysis based diagnostic accuracy (i.e. diagnostic accuracy obtained from validation session in the multiparametric analysis).

DISCUSSION

In the current study, several significant differences in univariate and multiparametric analyses using MR-derived quantitative parameters were obtained between local control and failure in patients with oropharyngeal or hypopharyngeal SCC treated by super-selective arterial infusions of cisplatin with concomitant radiotherapy. Our results in univariate analysis indicated that tumor sphericity and homogeneity were respectively revealed significant difference between local control and failure, whereas the value of TBF was revealed nearly significant although statistical significance was not obtained. Some studies previously investigated morphological (4, 23), intratumoral characteristics (4, 5), perfusion and diffusion information (9, 24) using medical imaging dataset in patients with pharyngeal SCC for predicting the treatment outcome, however, no study

Table 4. Detail of the training session

No. of session	Sensitivity	Specificity	PPV	NPV	Acuracy	Finally selected features
1	0.84	0.87	0.94	0.7	0.85	Sphericity, Homogeneity, TBF
2	0.89	0.75	0.89	0.75	0.85	Sphericity, Homogeneity, Surface area
3	0.84	0.87	0.94	0.7	0.85	Sphericity, Homogeneity, TBF
4	0.85	0.71	0.89	0.62	0.81	Sphericity, Homogeneity, TBF
5	0.84	0.87	0.94	0.7	0.85	Sphericity, Homogeneity, TBF
6	0.85	0.71	0.89	0.62	0.81	Sphericity, Homogeneity, TBF
7	0.84	0.75	0.88	0.66	0.81	Sphericity, Homogeneity, TBF
8	0.89	0.75	0.89	0.75	0.85	Sphericity, Homogeneity, TBF
9	0.84	0.87	0.94	0.7	0.85	Sphericity, Homogeneity, ADC
10	0.89	0.75	0.89	0.75	0.85	Sphericity, Homogeneity, TBF
11	0.84	0.87	0.94	0.7	0.85	Sphericity, Homogeneity, TBF
12	0.85	0.85	0.94	0.66	0.85	Sphericity, Homogeneity, TBF
13	0.84	0.87	0.94	0.7	0.85	Sphericity, Homogeneity, ADC
14	0.85	0.85	0.94	0.66	0.85	Sphericity, Homogeneity, TBF
15	0.84	0.87	0.94	0.7	0.85	Sphericity, Homogeneity, TBF
16	0.89	0.75	0.89	0.75	0.85	Sphericity, Homogeneity, ADC
17	0.89	0.75	0.89	0.75	0.85	Sphericity, Homogeneity, TBF
18	0.85	0.85	0.94	0.66	0.85	Sphericity, Homogeneity, ADC
19	0.84	0.87	0.94	0.7	0.85	Sphericity, Homogeneity, TBF
20	0.84	0.87	0.94	0.7	0.85	Sphericity, Homogeneity, Surface area
21	0.85	0.85	0.94	0.66	0.85	Sphericity, Homogeneity, TBF
22	0.84	0.75	0.88	0.66	0.81	Sphericity, Homogeneity, TBF
23	0.85	0.85	0.94	0.66	0.85	Sphericity, Homogeneity, TBF
24	0.84	0.87	0.94	0.7	0.85	Sphericity, Homogeneity, TBF
25	0.84	0.87	0.94	0.7	0.85	Sphericity, Homogeneity, TBF
26	0.89	0.75	0.89	0.75	0.85	Sphericity, Homogeneity, ADC
27	0.85	0.85	0.94	0.66	0.85	Sphericity, Homogeneity, TBF
28	0.84	0.87	0.94	0.7	0.85	Sphericity, Homogeneity, TBF

Table 4 footnote : PPV, positive predictive value : NPV, negative predictive value : tumor blood flow : ADC, apparent diffusion coefficient.

simultaneously evaluated all of these information using the same patient cohorts. In addition, our results indicated that a multiparametric approach-based diagnosis have a potential to predict the treatment outcomes more accurately than univariate approach. Especially, high sensitivity and positive predictive value to detect patients with the local control was obtained. The knowledge during the pretreatment period would be of great help to optimize the treatment regimen, for example regarding the need for additional chemotherapy such as induction therapy or possible earlier salvage surgery after current chemoradiotherapy. It would be also helpful to optimize the follow-up imaging strategy depending on the risk in each patient. Particularly, investigation related to imaging biomarkers for the outcome prediction in patients who received intraarterial chemotherapy was very limited ; our results may be useful information in the assessment for such patient population.

Related to the prediction of treatment outcomes using medical imaging dataset, as mentioned above, several studies have described the utility of tumor morphological information, tumor heterogeneity, and perfusion and diffusion information. The conventional morphological parameters of tumor volume and T-stage were reported to be predictive factors for the assessment of local control (25). In addition, several other studies investigated more advanced tumor morphological features compared to abovementioned conventional tumor volume information ; these studies reported that tumors with low 'sphericity' (i.e. high 'asphericity') were related to poor treatment outcome (4, 23). In addition, a recent analysis focused on intratumoral heterogeneity in the tumor depicted on medical imaging by calculating the second-order texture parameters reported that these parameters are independent indicators for the prediction of local control, and described tumors with highly heterogeneous intratumoral characteristics tended to result in poor treatment outcome (5). Tumor perfusion and diffusion have also been described as useful for the prediction of treatment outcomes as tumor functional information-reflecting parameters (9, 24), although pCASL and multiple b-value based DWI derived parameters were not statistically significant between treatment control and failure by univariate analysis in the current study. Our present study might accomplish the efficient selection of several features from various MR derived parameters and integrate them effectively to obtain the more powerful diagnostic algorithm. Multiparametric approach is an important diagnostic method with the selection of parameters efficiently and will continue to provide clinically usefulness. Several studies with this analytical approach providing clinical usefulness including the area of head and neck imaging were reported in recent years (14, 26, 27). However, the number of reports have exclusively focused on intratumoral characteristics such as second order texture parameters ; the utility of combined use including tumor shape information (e.g. tumor sphericity) and tumor functional information (e.g. tumor perfusion and diffusion) is still very limited. The analysis with initially assessing all of these information and efficient parameters selection may achieve higher diagnostic performance. In the current study, we preformed the multiparametric approach with the small number of finally selected parameters to avoid overfitting because our study cohorts in training dataset consisted of the small number of patients ; the sample size for training in multiparametric approach was generally considered at least 5-10 times the number of parameters used for the final diagnostic model (28). In addition, we initially used a relatively small number of imaging features (i.e., a total 16 MR-derived parameters) in creating the diagnostic model compared to conventional so-called radiomics studies which typically include hundreds of imaging features. As described above, the current study population was not large ; therefore, we analyzed a small number of imaging features to avoid inappropriate model creation due to overfitting and multicollinearity between imaging features ; such problems tend to be present in analyses with a small number of subjects and a large number of imaging features. Further study will be needed to reveal the presence of elevation in diagnostic performance by using all of tumor morphological, intratumoral characteristics, tumor perfusion and diffusion information with a larger number of study cohorts. Moreover, the validity of the current model needs to be assessed with the different cohort in the future study.

The present study has several limitations. First, the number of patients was small. We selected patient cohorts with availability of entirely MR-derived information, in addition, only patients who received the specific treatment regimen (i.e. super-selective arterial infusions of cisplatin with concomitant radiotherapy) were selected to avoid bias caused by different treatment methods ; these causes resulted in limited number of patients. As mentioned above, several studies suggested that tumor perfusion and diffusion can be useful in the prediction of treatment outcomes. However, pCASL- and DWI-derived parameters in the current study were not statistically significant in univariate analysis, although TBF obtained from pCASL and f from IVIM might have shown a tendency to predict local control/failure. We speculate that this was due to the small number of patients in the current study. Additionally, the specific treatment regimen used might have affected the results. Therefore, the results of the current study should be treated as preliminary, and further analysis with a larger number of patients is needed as described above. Second, the HPV status of some of the patients was not available. This status has a significant influence on prognosis and should be added to the multiparametric approach as an important parameter.

In conclusion, the multiparametric approach with the integration of several MR-derived tumor characteristics might have a possibility to become one of the supporting tools for the prediction of treatment outcomes. This diagnostic technique may contribute to the determination of the appropriate assessment for patients with oropharyngeal and hypopharyngeal SCCs.

CONFLICT OF INTERESTS-DISCLOSURE

None

ACKNOWLEDGEMENT

None

REFERENCES

1. Mizumachi T, Homma A, Sakashita T, Kano S, Hatakeyama H, Fukuda S : Confirmation of the eighth edition of the AJCC/UICC TNM staging system for HPV-mediated oropharyngeal cancer in Japan. Int J Clin Oncol 22 : 682-689, 2017
2. Pameijer FA, Mancuso AA, Mendenhall WM, Parsons JT, Mukherji SK, Hermans R, Kubilis PS : Evaluation of pretreatment computed tomography as a predictor of local control in T1/T2 pyriform sinus carcinoma treated with definitive radiotherapy. Head Neck 20 : 159-168, 1998
3. Coca-Pelaz A, Rodrigo JP, Suarez C : Clinicopathologic analysis and predictive factors for distant metastases in patients with head and neck squamous cell carcinomas. Head Neck 34 : 771-775, 2012
4. Fujima N, Hirata K, Shiga T, Li R, Yasuda K, Onimaru

R, Tsuchiya K, Kano S, Mizumachi T, Homma A, Kudo K, Shirato H : Integrating quantitative morphological and intratumoural textural characteristics in FDG-PET for the prediction of prognosis in pharynx squamous cell carcinoma patients. Clin Radiol 73 : 059.e1-1059.e8, 2018
5. Kuno H, Qureshi MM, Chapman MN, Li B, Andreu-Arasa VC, Onoue K, Truong MT, Sakai O : CT Texture Analysis Potentially Predicts Local Failure in Head and Neck Squamous Cell Carcinoma Treated with Chemoradiotherapy. AJNR Am J Neuroradiol 38 : 2334-2340, 2017
6. Truong MT, Saito N, Ozonoff A, Wang J, Lee R, Qureshi MM, Jalisi S, Sakai O : Prediction of locoregional control in head and neck squamous cell carcinoma with serial CT perfusion during radiotherapy. AJNR Am J Neuroradiol 32 : 1195-1201, 2011
7. Fujima N, Yoshida D, Sakashita T, Homma A, Tsukahara A, Tha KK, Kudo K, Shirato H : Usefulness of Pseudo-continuous Arterial Spin-Labeling for the Assessment of Patients with Head and Neck Squamous Cell Carcinoma by Measuring Tumor Blood Flow in the Pretreatment and Early Treatment Period. AJNR Am J Neuroradiol 37 : 342-348, 2016
8. Payabvash S : Quantitative diffusion magnetic resonance imaging in head and neck tumors. Quant Imaging Med Surg 8 : 1052-1065, 2018
9. King AD, Thoeny HC : Functional MRI for the prediction of treatment response in head and neck squamous cell carcinoma : potential and limitations. Cancer imaging 16 : 23, 2016
10. Rosenkrantz AB, Sigmund EE, Johnson G, Babb JS, Mussi TC, Melamed J, Taneja SS, Lee VS, Jensen JH : Prostate cancer : feasibility and preliminary experience of a diffusional kurtosis model for detection and assessment of aggressiveness of peripheral zone cancer. Radiology 264 : 126-135, 2012
11. Sun K, Chen X, Chai W, Fei X, Fu C, Yan X, Zhan Y, Chen K, Shen K, Yan F : Breast Cancer : Diffusion Kurtosis MR Imaging-Diagnostic Accuracy and Correlation with Clinical-Pathologic Factors. Radiology 277 : 46-55, 2015
12. Xu XQ, Ma G, Wang YJ, Hu H, Su GY, Shi HB, Wu FY : Histogram analysis of diffusion kurtosis imaging of nasopharyngeal carcinoma : Correlation between quantitative parameters and clinical stage. Oncotarget 8 : 47230-47238, 2017
13. Zhang B, He X, Ouyang F, Gu D, Dong Y, Zhang L, Mo X, Huang W, Tian J, Zhang S : Radiomic machine-learning classifiers for prognostic biomarkers of advanced nasopharyngeal carcinoma. Cancer Lett 403 : 21-27, 2017
14. Parmar C, Grossmann P, Rietveld D, Rietbergen MM, Lambin P, Aerts HJ : Radiomic Machine-Learning Classifiers for Prognostic Biomarkers of Head and Neck Cancer. Front Oncol 5 : 272, 2015
15. Li S, Wang K, Hou Z, Yang J, Ren W, Gao S, Meng F, Wu P, Liu B, Liu J, Yan J : Use of Radiomics Combined With Machine Learning Method in the Recurrence Patterns After Intensity-Modulated Radiotherapy for Nasopharyngeal Carcinoma : A Preliminary Study. Front Oncol 8 : 648, 2018
16. Kano S, Homma A, Oridate N, Suzuki F, Hatakeyama H, Mizumachi T, Furusawa J, Sakashita T, Yoshida D, Onimaru R, Shirato H, Fukuda S : Superselective arterial cisplatin infusion with concomitant radiation therapy for base of tongue cancer. Oral Oncol 47 : 665-670, 2011
17. Fujima N, Kudo K, Tsukahara A, Yoshida D, Sakashita T, Homma A, Tha KK, Shirato H : Measurement of tumor blood flow in head and neck squamous cell carcinoma by pseudo-continuous arterial spin labeling : comparison with dynamic contrast-enhanced MRI. J Magn Reson Imaging 41 : 983-991, 2015
18. Fujima N, Yoshida D, Sakashita T, Homma A, Tsukahara A, Tha KK, Kudo K, Shirato H : Intravoxel incoherent motion diffusion-weighted imaging in head and neck squamous cell carcinoma : assessment of perfusion-related parameters compared to dynamic contrast-enhanced MRI. Magn Reson Imaging 32 : 1206-1213, 2014
19. Fujima N, Sakashita T, Homma A, Shimizu Y, Yoshida A, Harada T, Tha KK, Kudo K, Shirato H : Advanced diffusion models in head and neck squamous cell carcinoma patients : Goodness of fit, relationships among diffusion parameters and comparison with dynamic contrast-enhanced perfusion. Magn Reson Imaging 36 : 16-23, 2017
20. Vujasinovic T, Pribic J, Kanjer K, Milosevic NT, Tomasevic Z, Milovanovic Z, Nikolic-Vukosavljevic D, Radulovic M : Gray-Level Co-Occurrence Matrix Texture Analysis of Breast Tumor Images in Prognosis of Distant Metastasis Risk. Microsc Microanal 21 : 646-654, 2015
21. Haralick R, Shanmugam K, Dinstein I : Textural features for image classification. IEEE Trans Syst Man Cybern 3 : 610-621, 1973
22. Kunimatsu A, Yasaka K, Akai H, Sugawara H, Kunimatsu N, Abe O : Texture Analysis in Brain Tumor MR Imaging. Magn Reson Med Sci (in press), 2021. doi : 10.2463/mrms.rev.2020-0159.
23. Apostolova I, Steffen IG, Wedel F, Lougovski A, Marnitz S, Derlin T, Amthauer H, Buchert R, Hofheinz F, Brenner W : Asphericity of pretherapeutic tumour FDG uptake provides independent prognostic value in head-and-neck cancer. Eur Radiol 24 : 2077-2087, 2014
24. Srinivasan A, Mohan S, Mukherji SK : Biologic imaging of head and neck cancer : the present and the future. AJNR Am J Neuroradiol 33 : 586-594, 2012
25. Ang KK, Harris J, Wheeler R, Weber R, Rosenthal DI, Nguyen-Tân PF, Westra WH, Chung CH, Jordan RC, Lu C, Kim H, Axelrod R, Silverman CC, Redmond KP, Gillison ML : Human papillomavirus and survival of patients with oropharyngeal cancer. N Engl J Med 363 : 24-35, 2010
26. Elhalawani H, Lin TA, Volpe S, Mohamed ASR, White AL, Zafereo J, Wong AJ, Berends JE, AboHashem S, Williams B, Aymard JM, Kanwar A, Perni S, Rock CD, Cooksey L, Campbell S, Yang P, Nguyen K, Ger RB, Cardenas CE, Fave XJ, Sansone C, Piantadosi G, Marrone S, Liu R, Huang C, Yu K, Li T, Yu Y, Zhang Y, Zhu H, Morris JS, Baladandayuthapani V, Shumway JW, Ghosh A, Pöhlmann A, Phoulady HA, Goyal V, Canahuate G, Marai GE, Vock D, Lai SY, Mackin DS, Court LE, Freymann J, Farahani K, Kaplathy-Cramer J, Fuller CD : Machine Learning Applications in Head and Neck Radiation Oncology : Lessons From Open-Source Radiomics Challenges. Front Oncol 8 : 294, 2018
27. Jethanandani A, Lin TA, Volpe S, Elhalawani H, Mohamed ASR, Yang P, Fuller CD : Exploring Applications of Radiomics in Magnetic Resonance Imaging of Head and Neck Cancer : A Systematic Review. Front Oncol 8 : 131, 2018
28. Sollini M, Antunovic L, Chiti A, Kirienko M : Towards clinical application of image mining : a systematic review on artificial intelligence and radiomics. Eur J Nucl Med Mol Imaging 46 : 2656-2672, 2019